A Polymer Model Explains MinDE Dynamics in *E. coli* Cell Division

Eric N Cytrynbaum* and Brandon Marshall†
Department of Mathematics, University of British Columbia
Vancouver, British Columbia, Canada

September 11, 2006

Abstract

In *Escherichia coli*, the location of the site for cell division is regulated by the action of the Min proteins. These protein undergo a periodic pole-to-pole oscillation that involves polymerization and ATPase activity of MinD under the controlling influence of MinE. This oscillation suppresses division near the poles while permitting division at midcell. Here, we propose a polymer model for MinD and MinE dynamics that is motivated by recent fluorescence, biochemical and genetic studies. The model quantitatively agrees with the experimentally observed dynamics in wild-type cells as well as a large set of mutant phenotypes, providing explanations for numerous phenotypes that have never been addressed by previous modeling attempts. Finally, the model emphasizes the importance of non-equilibrium polymer dynamics in cell function by demonstrating how behavior analogous to the dynamic instability of microtubules is used by *E. coli* MinD to achieve a sufficiently rapid time scale in controlling division site selection.

1 Introduction

Escherichia coli bacteria undergo division by pinching in half at the midpoint of the long axis of their cylindrical form. At the onset of this process, FtsZ, a bacterial homologue of tubulin, localizes to the inner membrane forming a polymer ring at midcell called the Z-ring. Along with a suite of other proteins, the Z-ring contracts, pinching the cell in two (see (1) for a recent review). The Z-ring is localized to midcell by the combined efforts of two independent pathways that suppress

*Corresponding author, email: cytryn@math.ubc.ca
†Email: bmarshal@interchange.ubc.ca

its polymerization. The first pathway is DNA-dependent and leads to the suppression of Z-ring formation in the regions immediately surrounding each of the two replicated and segregated chromosomes which sit on either side of the cell midplane. This leaves both the midcell and polar regions eligible for Z-ring formation (2). Polar division leads to asymmetric daughter cells, one containing two chromosomes and the other chromosome-less, and is referred to as a minicell phenotype. These polar divisions are usually suppressed in wild-type cells by the second pathway, the Min protein system – MinC, MinD and MinE. MinC is responsible for interfering with Z-ring formation (3, 4). MinD is an ATPase that localizes to the membrane in the ATP-bound form (5) and recruits MinC (6). MinE controls the spatial localization of MinD along the membrane (5) by inducing the ATPase activity of MinD (7). By restricting MinD and hence MinC to the polar regions, MinE spatially regulates the inhibition of division to the poles leaving only the midcell region available for Z-ring formation.

In *E. coli*, MinD and MinE act in a dynamic oscillatory manner that is independent of MinC (8). MinD first attaches to the inner cell membrane at one of the cell's two poles (8), then polymerizes in a tightly coiled helix extending from the originating pole almost to midcell (9). Subsequently, MinE attaches to MinD at the midcell end of the helix forming what was originally referred to as an E-ring (10) although a more recent microscopy study indicated that it might be better described as an E-helix (9). Upon attachment, MinE induces the ATPase activity of MinD (11) which drives the leading edge of the MinD helix back toward the pole. The E-ring progresses back toward the pole, clearing MinD as it goes (12, 13). MinD then reattaches at the opposite pole, repeating this pattern many times throughout the cell cycle with a period of roughly 40 seconds (8, 13).

Several mathematical models have been proposed to explain the MinDE oscillations as the spontaneous result of a Turing-like instability of a homogeneous protein distribution (14–18). Although spontaneous pattern formation of this kind has been observed in certain biopolymer systems (for example, (19–21)), it is more common for cells to employ dedicated proteins or structures that allow for precise spatiotemporal control of polymer nucleation. Examples include microtubule nucleation by γ-TuRC (22) and actin filament nucleation by Arp2/3 (23).

In contrast to these models in which both the spatial and temporal patterns arise spontaneously, it has been proposed previously that the spatial localization of MinD depends on specific anatomical features (24). In particular, domains of distinct lipid composition containing a high concentration of the anionic phospholipid cardiolipin have been observed at the poles of *E. coli* cells (25). Furthermore, a mutant lacking the cationic phospholipid phosphatidylethanolamine, having a membrane composed only of the anionic phospholipids phosphatidylglycerol and cardiolipin, was shown to have a loss of specificity in the localization of MinD, instead showing randomly scattered MinD foci (26). Norris et al. (2004) suggested that membrane lipid domains of distinct composition appearing at the poles might play a crucial role in division site selection. It was first thought that the ionic character of the lipids might increase the affinity of MinD for the poles but this effect was shown to provide at most an order of magnitude increase (26), arguably insufficient to explain the large polar bias in nucleation. Furthermore, this mechanism alone, which depends only on properties of MinD and the membrane, cannot explain the MinE dependence of polar nucleation (8, 27).

Here, we propose and quantitatively verify that sufficient amplification of MinD polar affinity can arise from the combination of two features: (i) a preference of MinD dimers for regions of membrane with low tension or curved membrane structures and (ii) the presence of such regions at the poles associated with lipid domains of distinct composition. While there is experimental evidence to support (i) and indirect evidence for (ii) (experimentally observed lipid domains of distinct composition (25) theoretically capable of inducing structural changes in the membrane (28)) direct evidence for (ii) is still lacking.

Another key feature of MinD that has been largely overlooked in the mathematical modeling literature is its membrane-associated polymer structure (9, 11, 29). Ignoring this structure fails to address the issue of whether spontaneous pattern formation is possible with a polymer paradigm which differs from the loose-aggregate paradigm that pervades the modeling literature. For example, the ability of individual MinD monomers to repeatedly cycle in and out of the same polar helix is described by Huang et al. (2003) as the mechanism by which the polar asynchrony of the oscillation is maintained in their model. However, this cycling is inconsistent with the fact that monomers attach and detach from a polymer at its tips only (30) raising concerns over the use of a non-polymer model to describe a fundamentally polymer phenomenon.

Of the numerous models that have appeared in the last few years, only one explicitly recognizes that the MinD polar helix is actually a polymer (31). In contrast with this previous model, the model presented here relies on detailed structural and biochemical data in formulating and justifying the assumptions, some of which are vital to understanding several MinE mutant phenotypes. It also exploits the fact that diffusion is a fast process relative to helix turnover and that only a single polymer forms at a time. With these simplifications, it admits a closed-form solution which provides a handle on parameter dependence and allows for quantitative validation against experimental data (8). The model also allows testing of the role and importance of cooperativity which has been reported in both MinD polymerization (11,32) and MinE hydrolysis-induction (11,29). Finally, the model allows for comparison with the many reported *min* mutant phenotypes including deletion of *minE*, overexpression of *minD* and *minE* in various combinations and at various expression levels, and three different truncations of the MinE protein also at various expression levels. Importantly, a majority of this mutant data has been unaddressed in the modeling literature until now.

From a more broad perspective, the model elucidates the role of non-equilibrium polymer dynamics in bacterial cell function. In the eukaryotic context, non-equilibrium behaviors like dynamic instability of microtubules and treadmilling of actin filaments have been shown to play vital roles in cell division, motility and other major functions. Here, we suggest that the MinD and MinE proteins together demonstrate behavior directly analogous to dynamic instability of microtubules and that this behavior is crucial to achieving Z-ring suppression at a sufficiently rapid rate.

2 The model

MinD dimer cycling and strain

We begin with a description of MinD dimer formation, a necessary precursor to polymer nucleation.

Upon binding ATP, MinD forms dimers (33) that attach to the inner membrane of the cell (11,34). Countering the MinD dimerization process, MinE also forms dimers in the cytosol (35) which can attach to the membrane-bound MinD dimers and induce hydrolysis thereby driving them off the membrane (11, 29) by a previously described mechanism (36, 37). This makes dimers a rare commodity on the membrane. Once in the cytosol, ADP is exchanged for ATP and the process can repeat. This cycle is illustrated in Figure 1.

We propose that this dimerization cycle is spatially regulated in the cell so as to facilitate nucleation exclusively at the pole in the following way. We claim that MinD-ATP dimers spontaneously bind to the membrane in a conformation that is strained provided the membrane resists deformation (flat membrane under tension). Furthermore, we assume that both strain and MinE attachment are required for inducing hydrolysis. One possible explanation for the strain requirement is that the strain is needed to close the dimerization face around the two ATPs, a conformation change that is thought to be an important step in the activation of several members of the structurally analogous ATPase family to which MinD belongs (38). Another possibility is that deformation associated with the strain might be required to allow MinE to bind, a scenario that is more consistent with the details of the calculation given in the Appendix.

From where does this hypothesis of strain in the dimer arise? In an *in vitro* membrane-binding assay, Hu et al. (2002) found that MinD-ATP, upon binding to lipid vesicles, was capable of distorting spherical vesicles of diameter $0.1 - 2$ μm into elongated tubes several microns in length with an approximate radius of $r = 25$ nm. Furthermore, from diffraction patterns of cryo-EM images of tubes, they observed that MinD formed a lattice encircling the tubes on the outside with a lateral spacing of about the width of a MinD monomer. This suggests that upon attaching to lipid vesicles, not only does MinD-ATP form a polymer structure but this structure has an energetic preference to take on a curved conformation when attached to membrane. In other words, membrane-associated MinD polymerization provides a force with which membrane is deformed and a membrane tube is pulled from a vesicle, a phenomenon similar to that observed for dynamin (39) and microtubules (40) as well as studied with techniques using glass beads (41).

Next we use the details of this *in vitro* observation to estimate the energy associated with dimer strain. We assume the following time course for the vesicle tubulation phenomenon, illustrated in Figure 2. At sufficiently high concentrations of MinD, a polymer forms on the surface of the vesicle pinching out a tube thereby removing any membrane area stored in undulations. Based on the extent of tubulation observed (11), we further assume that MinD is capable of pulling the membrane tube into the regime in which the membrane is stretched.

For any observed length of polymer tube l in the membrane-stretching regime, we can calculate the stretching energy required to extend the tube by a length Δl. Initially, not much energy is required for extension but when l reaches 400 nm, the change in energy stored in membrane stretching through elongating the tube by one loop of 25 dimers ($\Delta l = 6$ nm) is around 180 k_BT which amounts to just over 7 k_BT per dimer (see Appendix for details). Note that it is possible that the membrane is ruptured during the process (see (11)). However a 400 nm long tube pulled from a 400 nm radius vesicle represents a percentage stretching of about 1.2% which is below the range of membrane rupturing (42) so rupture would not occur within the range relevant to the

calculation presented here.

This calculation indicates that when attached to a flat, high tension membrane that does not permit deformation, a MinD polymer is forced to deform and can store this energy as mechanical strain internal to the polymer itself. We assume that the strain is present at the dimer level.

Polar nucleation of MinD polymers

In the appropriate membrane environment, MinD dimers would fail to maintain strain, thereby slowing or stalling MinE-induced hydrolysis and, in turn, MinD release from the membrane. An environment of this type could well exist at the cell poles, associated with a known domain of distinct lipid composition (25) which could theoretically cause changes in membrane curvature or tension (24, 28). A slower rate of hydrolysis at the poles would lead to an accumulation of dimers and therefore a much increased probability of nucleating a MinD helix at the poles compared to elsewhere on the membrane, as is characteristic of wild-type cells (8).

Calculations provided in the Appendix demonstrate that the lack of strain alone at the poles leads to a 2-3 order of magnitude difference in the concentration of MinD dimers at the poles compared with elsewhere on the membrane. This means that the probability of nucleating a MinD polymer anywhere other than at the poles is much reduced.

Cooperativity and tension-based exclusion of nucleation

In addition to being relegated to the poles, nucleation is cooperative in the sense that the polymer nucleation rate proportional to D^n where D is the cytosolic concentration of MinD and $n = 3$ or 4 (see Appendix). Here we are assuming that the MinD helix is formed by a single double-stranded polymer, an assumption justified by concentration and geometric constraints (see Appendix). This non-linear nucleation probability is typical of multi-stranded polymers (e.g. $n = 3$ or 4 for actin filaments (43), $n = 12$ for microtubules (44)).

Cooperativity of this type has been observed in *in vitro* MinD-membrane-binding assays (11,32). This means that as a MinD polymer is disassembling at one end, a polymer can only form at the other pole once a sufficient fraction of the polymer has disassembled, an important feature for maintaining the asynchrony of polymer growth at either pole. Also, the delay between disassembly at one end and assembly at the other means that both diffusion and ATP-ADP exchange have a significant period of time over which to occur, up to half of the oscillation period, so it is reasonable to assume that both are quasi-steady processes with respect to assembly and disassembly dynamics (see Appendix for details).

Another important feature of nucleation is that once a first polymer forms at one pole, other polymers are inhibited from forming at the same pole due the membrane tension induced by the growth of the first polymer. Accumulation of dimers would no longer be preferred at the occupied pole due to the higher membrane tension induced by pulling out the membrane tube.

MinE and E-ring formation

MinE monomers have three distinct structural features that are important in the discussion of their role in division site selection, the anti-MinD domain, the dimerization residues and the topological

specificity residues (depicted in Figure 1). The anti-MinD domain sits at the N-terminus of the protein (residues 1-32) and consists primarily of an α-helix. It is known to be necessary and sufficient for driving MinD from the membrane (45, 46). Dimerization depends on the interaction of several portions of the C-terminus domain of the protein (residues 33-88) which together form a β-sheet and coiled-coil in the assembled dimer (47). Finally, the topological specificity (TS) residues, 45 and 49 (and possibly some neighboring ones), are required for MinE to selectively target its anti-MinD activity to MinD in the midcell region. Loss of these residues leads to a failure to form the E-ring (48). We assume these residues play a role in binding of MinE to membrane-bound MinD, as suggested by Shih et al. (2002). This assumption is also supported by evidence that when the anti-MinD domain is prevented from binding to MinD, MinE is still capable of binding to membrane-bound MinD, despite being incapable of inducing ATPase activity (49). Based on the location of the TS residues on the C-terminus α-helices (light patches on the underside of MinE in Figure 1(A)) (47) and a matching of the geometries of the MinD and MinE dimers, their binding is assumed to occur as depicted in Figures 1 and 3.

An important issue to address is the mechanism by which MinE influences the ATPase activity of MinD dimers. In comparison with a structurally analogous ATPase involved in nitrogen fixation (NifH), MinD is missing an α-helix at the edge of its dimerization face (38) (see Figure 3(B)). Here, we propose that this missing α-helix is required for ATP hydrolysis and is replaced in the MinD context by the anti-MinD domain of MinE. This idea is consistent with the finding that the anti-MinD domain interacts with the so-called α-7 helix (the yellow α-helix in Figure 3(B)) (50) and that mutations in α-4 (the green α-helix in Figure 3(B)) and α-7 suppress the influence of MinE on MinD ATPase activity (49, 51) (this α-helix nomenclature is adopted from (52)). The assumption is that upon attaching to MinD, the anti-MinD domain of MinE must rotate into place near the dimerization face and, by interacting with α-4 and α-7, induces hydrolysis (see Figure 1(v)). Finally, cytosolic MinE monomers and dimers are both assumed to be capable of clearing the non-polar membrane of MinD dimers. The MinE dimer structure does not seem necessary for this membrane clearing activity based on the fact that a truncated form of MinE that is missing the dimerization domain is nonetheless capable of inducing MinD-ATP hydrolysis (45).

The next important issue to address is the manner in which MinE effects the MinD polymer, which generally ceases growth and begins disassembly at its midcell tip upon formation of the E-ring (12, 13). *In vitro* studies have shown that MinE is capable of forming tertramers in solution at extremely high concentrations (K_D = 2mM) (35). *In vivo*, we propose that MinE polymer formation is facilitated at lower concentration by the framework of the MinD polymer to which MinE can attach. Thus we describe the E-ring as a "retrograde" double-stranded polymer that sits on top of the MinD polymer. E-ring formation guarantees that disassembly of the MinD polymer is processive – as a MinD dimer hydrolyzes its ATP and falls off the membrane, the next MinE down the line rotates its anti-MinD domain into place. The E-ring treadmills back along the MinD helix, preventing further growth and inducing disassembly.

In principle, the E-ring could nucleate at any point along the MinD polymer through attachment of three neighboring monomers via their TS residues. However, the added affinity for MinD provided by the anti-MinD domain biases E-ring formation to the tip of the MinD polymer, the

only location at which α-7 is accessible to the anti-MinD domain (see Figure 3). There are two pathways by which the E-ring can nucleate, either by sequential binding of two monomers at the tip or by the binding of a single dimer. The monomer pathway can be interrupted either by spontaneous dissociation of the first MinE monomer or by its induction of hydrolysis by its MinD host which would lead to its own release. In contrast, the dimer pathway does not have this intermediate limiting step but instead requires dimerization in the cytosol before attaching to the tip. In either case, it can be argued that both tip-binding pathways, including the addition of a third monomer, occur at a rate proportional to the cube of the cytosolic monomer concentration but with different coefficients. Because of the limiting intermediate step in the monomer pathway, we argue that the monomer pathway is marginal and so omit it from the model. Cooperativity of MinE ATPase induction has been observed *in vitro* (11,29) and we infer that it is of the second type – cooperativity through cytosolic dimerization rather than facilitated binding to the MinD polymer.

This argument means that E-ring nucleation awaits the arrival of sufficient MinE dimers in the cytosol. Zhang et al. (1998), measured an *in vitro* dissociation constant for dimerization of $K_D = 0.6\mu$M well within the *in vivo* range. We therefore propose that the cytosolic concentration of MinE dimers is dynamically controlled during the MinDE oscillations so that E-ring nucleation happens *after* the MinD polymer grows far enough toward midcell to inhibit polar division. This control is accomplished by sequestration of cytosolic MinE in the E-ring attached to the older disassembling MinD polymer.

To summarize, suppose that one MinD polymer is already capped by an E-ring and a second polymer has just formed. As a MinD-MinE dimer pair pop off the tip of the first polymer, the liberated MinD, following ATP-ADP exchange, can incorporate into the nascent polymer but is blocked from incorporating into the older disassembling polymer by the anti-MinD domain at its newly exposed tip. But why should the liberated MinE dimer rebind to the same E-ring (E-ring treadmilling) and not contribute to the formation of an E-ring on the nascent second polymer? This question is important because, if it did, the nascent polymer would be capped early allowing for assembly of the division apparatus near the pole and hence minicelling. Because an E-ring already exists on the older polymer, much of the cytosolic pool of MinE is sequestered in that ring and the cytosolic concentration is low, in particular below K_D, so that most of the cytosolic pool is in monomer form. Monomers don't initiate E-rings but they can readily elongate existing ones, an important feature of multi-stranded polymers (30). It is only when the E-ring covers the length of the shrinking MinD polymer that monomers can no longer add to it, leading to a rise in the total cytosolic MinE concentration and in turn the dimer concentration. This finally triggers E-ring nucleation on the nascent polymer. This behavior, combined with the cooperativity of MinD polymer nucleation, is the source of stable asynchrony in the MinDE oscillations.

Equations and parameters

The model equations include one equation for the length in μm of each MinD polymer (left, $l(t)$ and right, $r(t)$) and each E-ring ($l_E(t), r_E(t)$). When not capped by an E-ring, MinD polymer growth is proportional to the cytosolic concentration of MinD (D) and while an E-ring is attached, disassembly progresses at a constant rate:

$$\text{No E-ring: } \frac{dl}{dt} = \frac{\delta}{2} k_{on} D, \quad \text{with E-ring: } \frac{dl}{dt} = -\frac{\delta}{2} k_{off},$$

Identical equations hold for the right polymer. Diffusion is fast relative to other time scales (see Appendix) so D is found simply by conservation of monomers:

$$D(t) = D_{tot} - \frac{2}{600 V \delta}(l(t) + r(t))$$

where δ is the diameter of a MinD monomer in μm, V is the volume of the cell in μm^3 and the 600 accounts for the conversion from monomers per μm^3 to μM.

Once an E-ring has formed, for example on the left MinD polymer, the following equation describes its growth:

$$\frac{dl_E}{dt} = \frac{\delta}{2}\left(k_{on}^E E H(l - l_E) - k_{off}\right)$$

where H is the Heaviside function (the E-ring can grow no longer than the MinD polymer on which it sits). As with MinD, conservation and rapid diffusion allow the cytosolic monomer concentration to be found by solving

$$E + 2E_2 + \frac{2}{600 \delta V}(l_E + r_E) = E_{tot}$$

where E is monomer concentration and $E_2 = E^2/K_D$ is the dimer concentration, assumed to be in quasi-static equilibrium with E.

Transitions between the deterministic dynamics of polymer growth and polymer disassembly (MinD nucleation and E-ring formation) can be treated in two ways. A fully deterministic approach implements nucleation and capping as strictly concentration-dependent threshold events which amounts to exaggerating the cooperativity of dimer formation for both MinE and MinD. That is, as the cytosolic MinD concentration rises above a threshold level, D_{thresh}, an empty pole spontaneously nucleates a polymer. Similarly, if the cytosolic MinE dimer concentration surpasses a threshold value, E_{thresh}, a growing polymer is capped with an E-ring. We implicitly assume that the formation of the E-ring both induces processive hydrolysis at the polymer tip and prevents further MinD polymerization. Under the assumption that both MinD and MinE polymer growth are at quasi-steady state, the equations are solvable in closed form (see Appendix).

The second implementation treats MinD nucleation and E-ring formation as stochastic events where the probability density of either event is taken to be $k_{nuc} D^n$ and $k_{cap} D^m$ respectively where n and m are either 1 or 3. The cubic case is more realistic, as described above, but the linear case is included to demonstrate the importance of the cooperativity which arises through dimerization. Also, $n = 4$ is arguably more likely based on concentration estimates (see Appendix) but we use $n = 3$ as a conservative estimate. Cases $\{n = 3, m = 3\}$, $\{n = 1, m = 3\}$ and $\{n = 3, m = 1\}$ are all described in the Results section.

Parameters values for both implementations are listed in Table 6. A more detailed discussion

of parameter values is provided in the Appendix.

3 Results

MinDE oscillations

In the deterministic implementation of the model, two relevant solutions can be calculated. Provided $D_{tot} - D_{thresh} > E_{tot} - E_{thresh}$, a stable oscillatory solution reminiscent of wild-type oscillations can be found (see Appendix and Figure 4). This condition is equivalent to enforcing that the cytosolic MinD nucleation threshold must be reached before the cytosolic E-ring forming threshold is reached as a MinD polymer and E-ring disassemble. When this condition is not satisfied, a purely cytosolic state prevails – MinD polymers are capped and disassembled before they even have a chance to grow – and a minicell phenotype is predicted. In Figure 4, this condition is illustrated by the fact that the nucleation threshold is higher than the capping threshold (shown graphically in terms of polymer length instead of cytosolic concentration).

When the oscillation condition holds, the period of the oscillations is given by $T = 1200V(D_{tot} - 2(E_{tot} - E_{thresh}))/k_{off}$ (see Appendix). This translates into the time it takes to disassemble a maximal MinD polymer (i.e. one using all monomers) less twice the time it takes to disassemble the MinD polymer remaining at the moment a new polymer nucleates. Interestingly, this expression demonstrates that the time scale of the process is determined solely by the disassembly rate, E-ring initiaition threshold, total concentrations and cell size but not the nucleation threshold nor the assembly dynamics. The latter two parameters only determine the fraction of the oscillation period that the polymer spends growing.

With parameter values as given in Table 6, the oscillation condition is satisfied and the predicted oscillation period is 45 seconds, roughly consistent with observations (8,13). Not appearing in the expression for the period, D_{thresh} is only restricted to a broad range of values by the oscillation condition, 0-3.5 μM, consistent with *in vitro* evidence which places it the range 1.5-3 μM (11).

Cooperative nucleation and dimer-driven E-ring formation generate robust MinDE oscillations in wild-type cells

The stochastic-transition version of the model was implemented numerically to test the robustness of the model with respect to cooperativity. In the deterministic case, exaggerated cooperativity (i.e. sharp thresholds) lead to guaranteed oscillations - to what extent is cooperativity required? In the stochastic case, cooperativity was implemented by treating the probabilities of nucleation and capping as proportional to either the concentration of MinD and MinE respectively (no cooperativity) or the cube of these concentrations (cooperativity).

Interestingly, cooperativity of nucleation is not essential to the oscillations. When the probability of nucleation is taken to be a linear function of MinD concentration instead of a cubic function, MinD helices still form in an alternating manner provided the nucleation rate is sufficiently high. However, the fidelity of polymer alternating between the poles is not as high in this case. For the cooperative case, in a simulation lasting 1600 seconds, there were 5 skipped beats (i.e. a polymer

appearing twice in immediate succession on the same pole) out of 118 nucleation events whereas in the non-cooperative case, there were 23 skipped beats out of 133 nucleation events. Note that although the simulations demonstrate that a nucleation rate which is linear in cytosolic concentration is sufficient to ensure oscillations, the model implicitly assumes that nucleation occurs uniquely at the poles, an assumption that relies on the dimer-cycling modeled outline above.

Even more remarkable is the fact that the MinE dimer mechanism proposed in this paper is not essential for the oscillations either, contrary to our expectations. When the probability of E-ring initiation was taken to be a linear function of MinE monomer concentration rather than a cubic function, oscillations were almost as consistent as for the cooperative model (8 skipped beats out of 113 nucleation events in 1600 seconds). However, there was a marked increase in the variability in the time between the onset of E-ring disassembly on one MinD polymer and the moment of E-ring initiation on the nascent distal MinD polymer. This interval of time was measured to be 7.1 ± 4.3 seconds for the cubic function case and 7.1 ± 7.0 seconds for the linear case. The extreme variability observed was anticipated but it was expected to lead to a complete failure in the polar alternation of polymerization. This was not the case.

In this study, we consider only whether the polymer undergoes a relatively consistent alternation from pole to pole. If a more careful analysis were carried out, for example checking for the presence of temporal gaps in the polar localization of MinD long enough to allow FtsZ to form a Z-ring at a MinD-less pole, these non-cooperative cases would likely generate higher rates of minicelling than seen in wild-type cells.

A qualitative sense of the difference between the cooperative and non-cooperative regimes can be gained from Figure 6. Note that parameter values in the non-cooperative cases are identical to those in the cooperative case except that, for non-cooperative nucleation, the nucleation rate is taken to be an order of magnitude larger than in the cooperative case and for the non-cooperative E-ring case, the E-ring initiation rate is taken to be an order of magnitude lower. As well, for the non-cooperative E-ring case the cytosolic MinE pool is assumed to be entirely in monomer form, consistent with the absence of cooperativity in the form of dimerization.

Across all model variations simulated, including all four permutations of cooperative and non-cooperative MinD nucleation and E-ring formation, the measured statistics other than those already mentioned were approximately the same. For example, the oscillation period was roughly 50 ± 20 seconds in all cases. Also, the maximal fraction of the cell covered by polymer was $\approx 34\% \pm 13\%$ which is in good agreement with observations (48).

Mutants

Directed mutant studies (reverse genetics) offer a powerful tool for exploring the different roles played by distinct domains of a single protein. Such studies also provide an effective way of testing a model. With the *min* system, much work has focussed on overexpression, deletion, truncation and point mutations of the MinE protein. In this section, we describe the widespread agreement between the mutant phenotypes and the corresponding predictions that arise from the proposed model.

Cells lacking MinE (*minE*$^-$) show a uniform membrane localization of MinD.

In the absence of MinE, MinD appears to associate with the membrane but fails to nucleate polymers (8,27). This is counter-intuitive as MinE is known to inhibit the association of MinD with the membrane but it is also apparently necessary for polymerization. The paradox is easily resolved by the dimer cycling model. Without MinE, the polar and non-polar membrane concentrations of MinD are much closer to each other and relatively low in comparison with wild-type cells wherein polar concentrations are predicted to be 2-3 orders of magnitude higher than elsewhere. We estimate that a nucleation threshold of 250-500 dimers/μm^2 would allow nucleation only at the poles in wild-type cells and nowhere in the mutant (see Appendix). In different contexts, this polymer-less phenotype causes either minicelling (8,27) or a complete block of division (5,27). We infer that the difference between these two cases depends on the expression level of MinD. At low concentrations, membrane-bound dimers are unable to recruit sufficient MinC to suppress Z-ring formation whereas at higher concentrations, enough MinC is recruited and is recruited uniformly across the cell leading to suppression of division everywhere.

Overexpression of *minE* and *minD*.

Over-expression studies have demonstrated that the total concentrations of both MinD and MinE have an influence on phenotype and, in particular, when MinD still undergoes wild-type oscillations, on the period of the oscillation. Using the available data, estimation of parameter values is possible. The goal is not to demonstrate that the model can accurately match specific experimental measurements but is rather to demonstrate that the model can be made consistent with a range of phenotypes and captures quantitative trends in the experimental data.

We focus on a subset of the observations of Raskin and deBoer (1999a) for which the oscillation condition and the expression for oscillation period T are valid (see "MinDE Oscillations"). Each of the following described experiments was carried out by introducing a λ phage to express the desired protein(s). We assume that for each protein, expression levels are the same but, as with the endogenous proteins, other factors lead to a 4:3 ratio in the concentration of MinD to MinE (48).

Wild-type cells were found to oscillate with an average period of 38 seconds. Over-expression of *minD* in a wild type background showed wild-type division patterns but it was found that the MinD oscillations have a period of 96 seconds, significantly longer than unperturbed cells. Interestingly, simultaneous over-expression of both *minD* and *minE* in a wild type background returns the oscillations to normal periodicity (40 seconds) (8). Expression of both *minD* and *minE* in a Δ*minCDE* mutant failed to rescue the minicelling seen in Δ*minCDE* cells but oscillations of a period similar to wild-type cells were reported (8). In later experiments, it was found that higher expression levels of *minD* and *minE* were able to restore the wild-type phenotype including the oscillation period in the Δ*minCDE* mutant (13).

All of these data can be explained by the model. Equating the experimental values for oscillation periods with the derived expression for the period, replacing D_{tot} and E_{tot} by $D_{tot} + \lambda$ or λ and $E_{tot} + \frac{3}{4}\lambda$ or $\frac{3}{4}\lambda$ when appropriate, gives a system of four over-determined equations in terms of the unknown parameters E_{thresh}, the E-ring-formation threshold and λ, the level of exogenous expression. A least squares fit provides values of $E_{thresh} = 2.5\mu$M and $\lambda = 3.3\mu$M such that the predicted periods are roughly consistent with those reported in (8) (see Table 2). In addition, the fact that $\frac{3}{4}\lambda \sim E_{thresh}$ means that when *minDE* is expressed in a Δ*minCDE* cell at a level λ, there

is just barely enough MinE to initiate an E-ring. Thus under stochastic variations, E-rings might occasionally fail to form thereby delaying the oscillations and allowing for polar Z-ring formation. This offers a possible explanation for the observed minicell phenotype. At higher MinE expression levels, E-ring formation would not be a problem, which is consistent with the later observation that higher expression levels rescued the minicell phenotype. The predicted value of λ is therefore considered to be and is henceforth referred to as "low" relative to wild-type levels.

The analytical solution also allows for the estimation of the maximum percentage coverage of the cell length by the MinD polymer (included in Table 2 and visible in Figure 4 as the maximum height at $t = 0$ and $t = t_{cap}$) and the length of time during which different cell locations are exposed to Z-ring formation (unshaded zones in Figure 4), both useful in understanding two other experiments. Intermediate levels of *minD* over-expression in a wild type background causes minicelling and at yet higher levels, complete block is seen (8). Notice that even at low levels of *minD* over-expression, the MinD helix is predicted to cover 78% of the cell when at its maximum length. This means that the midcell region is exposed to FtsZ for only a brief portion of the oscillation, ~ 25 seconds for the parameters in Table 6, whereas the poles are exposed for only ~ 15 seconds. At intermediate levels of exogenous expression ($\lambda \sim 5.3\mu$M instead of 3.3μM), the window of opportunity for Z-ring formation closes down completely at midcell. However, there is ~ 20 seconds of exposure at the poles coincident with a lengthening of the oscillation period (150 seconds) so minicelling is a more likely option. For higher expression levels ($\sim 7.3\mu$M), a polymer originating at either pole reaches all the way across to the opposite pole (predicted maximal coverage of 110%) thereby shutting down all options for Z-ring formation which explains the observed complete division block.

Another related phenotype is the over-expression of *minE* in a wild type background which causes minicelling (5). This can be explained by the oscillation condition in that if the right hand side of the inequality is increased by more than 0.5-2 μM (depending on the exact value of D_{thresh}) above wild-type values, the condition is no longer satisfied (hence minicelling).

Minicelling with (i) a truncated form of MinE ($\mathbf{MinE^{1-22}}$), and (ii) a two-point-mutation, $\mathbf{MinE^{D45A/V49A}}$

These two cases are similar in the sense that both are characterized by having an anti-MinD domain that is incapable of being correctly localized to a MinD polymer tip due to lack of (functional) TS residues. In the case of MinE^{1-22}, the entire protein consists only of the anti-MinD domain and is missing the TS residues which are essential for MinE to properly control MinD localization (45). The other, $\mathrm{MinE}^{D45A/V49A}$, has had the TS residues mutated and has been shown to be incapable of forming E-rings (48). Due to the predicted similarity between these two mutants, only $\mathrm{MinE}^{D45A/V49A}$, for which GFP fusions have been made and studied (48), is described here.

The $minE^{D45A/V49A}$ phenotype at the level of fluorescence observations was described in detail by Shih et al. (2002). In contrast with the complete absence of MinE, cells with MinE replaced by $\mathrm{MinE}^{D45A/V49A}$ are still capable of MinD polymerization. In the context of our model, this means that the hydrolysis-inducing domain of $\mathrm{MinE}^{D45A/V49A}$ is still capable of clearing MinD dimers from the non-polar regions of the membrane even without functional TS residues.

However, $\mathrm{MinE}^{D45A/V49A}$ was found to differ from wild-type MinE in several ways other than the lack of E-rings. MinD helices were seen to extend further than in wild-type cells, often reaching

beyond midcell. MinD disassembly occurred but in a disrupted manner, sometimes stuttering with an assembly phase interspersed with disassembly and often reaching all the way to the opposite pole with subsequent disassembly starting from either pole after a "highly variable time". In filamentous cells, internal MinD zones were seen sometimes treadmilling from one end of the cell to the other, sometimes growing at both ends and sometimes shrinking at both ends. In general, disassembly was significantly slower than in wild-type cells with typical times scale for disassembly in the range of 5-15 minutes (48)). In addition to these fluorescence observations, minicelling was observed.

To explain this erratic phenotype, we make the assumption that although incapable of attaching stably to MinD, $\mathrm{MinE}^{D45A/V49A}$ is nonetheless capable of inducing MinD ATPase activity upon encountering a MinD tip at the membrane. Importantly, its activity is not processive along the MinD polymer as it would be if an E-ring could be formed, nor is there ever a consistent impediment to polymer assembly. This means that the polymer length undergoes a random walk with monomer addition and hydrolysis-induced removal randomly interspersed. The diffusion coefficient of such a random walk is roughly $k_{off}(\delta/2)^2 \sim 5 \times 10^{-4} \mu\mathrm{m}^2/\mathrm{s}$ (30) giving a predicted average lifespan for a MinD helix initially 1 μm long of about 17 minutes. This process can explain all of the observed characteristics.

The longer-than-wild-type MinD helices can be explained by the fact that without E-ring formation, there is no arrest of helix growth. The appearance of stuttering is a direct manifestation of the random walk. The highly variable time required for release of one of the tips of a full-length MinD polymer stems from the stabilization of the polymer at both poles which slows the random walk leading to a delayed and highly variable escape time. The slow diffusive disassembly of the MinD polymer at one pole leaves the other poles empty for long enough for a Z-ring to form thereby leading to minicelling. The treadmilling, growing and shrinking MinD zones seen in filamentous mutants can be explained as well. With transitions from assembly to disassembly and vice versa occurring randomly, a MinD polymer with two tips would spend time in all four possible states (assembly at both ends, disassembly at both ends and treadmilling in either of two directions). The overall slowing of disassembly is consistent with the 17 minute estimate for the average lifespan of a polymer.

Several complication exist. A diffusive process would not have distinct periods of assembly and disassembly although with a large sampling interval, this might not be distinguishable. Furthermore, the random walk here is biased by the asymmetry of assembly, which is dependent on cytosolic MinD concentration, and disassembly, which is not. This would allow for periods of processive assembly. In contrast, given the longer time scales of diffusive disassembly, ATP-ADP exchange may play a significant role leading to periods of processive disassembly. Thus, subject to the subtleties of these unresolved details, all the $\mathrm{MinE}^{D45A/V49A}$ phenotypes described by Shih et al. (2002) are feasible within the scope of this model.

Wild-type cells with expression of a MinE^{22-88} fragment

Expression of the 66 C-terminus amino acids of MinE in an otherwise wild-type cell at levels comparable to the wild-type MinE protein results in a minicell phenotype (35). In deciphering this phenotype, it was shown that MinE^{22-88} can form homodimers as well as heterodimers with MinE (35). What does this mean in the context of the polymer model? Assuming dimerization

occurs at random, roughly 25% of dimers would be MinE homodimers, 50% would be heterodimers and 25% would be $MinE^{22-88}$ homodimers. With all three types of dimers having an intact TS domain, an E-ring initiated by one of the first two types but composed of all three should form. With twice as many total dimers available, the E-ring would be longer than usual (keeping total cytosolic dimer concentration at E_{crit}) and should therefore begin to disassemble earlier than usual, as with overexpression of wild-type MinE. However, despite the possibility of early E-ring formation, during E-ring treadmilling one out of every two dimers would be incapable of inducing MinD hydrolysis whether due to a heterodimer with its sole anti-MinD domain facing away from the tip or due to a $MinE^{22-88}$ homodimer with no anti-MinD domain at all. This would cause a stuttering in the disassembly, allowing cytosolic MinD to attach at the tip and possibly destabilizing the E-ring. Without E-ring processivity, the MinD-less pole would be left for extended periods of time unprotected from Z-ring formation thereby allowing minicelling.

When $MinE^{22-88}$ is expressed at much higher levels, so high that essentially no wild-type homodimers form (as determined by immunoblotting), a complete block of division is seen (35). An independent study showed that mutations to MinD's α-7 α-helix allows MinC to outcompete MinE which is not its normal behavior (49). A mutation to α-7 on MinD is in some sense equivalent to a loss of the anti-MinD domain on MinE because these domains are known to interact (50). Provided MinC can outcompete the heterodimers which would theoretically have an affinity for MinD somewhere between that of wild-type and mutant homodimers, this competition would severely limit the dimer cycling required to concentrate the MinD dimers at the poles and simultaneously lead to a complete block of division. This problem would not arise at the lower expression level because of the presence of wild-type homodimers.

Interestingly, expressing a slightly shorter protein, $MinE^{36-88}$, in wild-type cells also causes minicelling however this phenotype persists over a wide range of concentrations and does not transition to a division-failure phenotype at high concentrations as seen with $MinE^{22-88}$. The difference between these two truncations is that $MinE^{36-88}$ monomers are incapable of forming heterodimers with wild-type monomers and presumably homodimers with itself (35). This truncation is apparently missing only part of the dimerization domain as it still retains a pair of β sheet strands and a coiled coil involved in dimerization (47). First, the transition to complete division block would not occur here because the only dimers to form would be wild-type homodimers. The fact that the debilitated protein is able to cause minicelling stems from the fact that although monomers are unable to initiate an E-ring, they can still elongate an existing E-ring. Even if $MinE^{36-88}$ is incapable of dimerizing in the cytosol, it might still be able to bind as a monomer to the E-ring and subsequently dimerize under the stabilizing influence of the MinD polymer and existing E-ring. Once incorporated into the E-ring, the truncated protein would have the same processivity-reducing influence on MinD helix disassembly as described for the longer fragment.

4 Discussion

In this paper, we have put forward several new ideas, wrapped in the framework of a quantitative model, in order to link a broad range of experimental results across several scales from protein structure to cellular phenotype.

The combination of a MinD-ATPase cycle, spatially modulated by protein mechanics, in the context of inhomogenous membrane tension provides an explanation for the observed polar bias and cooperativity of MinD polymer nucleation. An important feature of this component of the model is that it does not rely on a spatially graded membrane affinity of MinD in isolation. Instead, MinD attachment to the membrane is homogenous but the detachment rate is MinE-dependent in a spatially graded manner. We propose that lower MinE activity at the poles is due to a lack of strain in the MinD dimer but this is only one possibility which illustrates the principle. Independent of the details of the mechanism, the general principle simultaneously accounts for nucleation at the poles in wild-type cells and a lack of nucleation in the $minE^{-}$ mutant.

The details of MinE protein structure motivates the major assumptions underlying this protein's roles in division site selection. The anti-MinD domain plays the dual role of hydrolysis induction and suppression of MinD polymer growth through steric exclusion at the polymer tip. The TS residues allow for the formation of the E-ring which imparts processivity to the MinE-induced disassembly and delays formation of the next E-ring by cytosolic depletion of MinE. Finally, concentration-dependent dimerization in the cytosol via the C-terminus α-helix and β-sheet is also necessary to properly control the timing of E-ring formation. Together, these component parts impose on the MinD polymer two distinct states, an assembly state and a disassembly state, through which correct division site selection is rapidly accomplished, as discussed in more detail below. The large set of mutant studies provide a clear means of testing out the details of these proposed roles; the mathematical model successfully provides a connection between protein function at the molecular scale and the emergent phenotypes at the cellular scale in all cases discussed.

"Dynamic instability" of MinD provides a sufficiently rapid means of suppressing polar division.

Dynamic instability of microtubules has been described as a means by which a cell can rapidly search through intracellular space. Theoretical estimates of capture time for chromosomes during prometaphase in eukaryotic cells showed dynamic instability to be more efficient than reversible polymerization which proceeds by interspersed addition and removal of monomers (53). For *E. coli*, the difference between these two modes of polymer dynamics is clearly demonstrated by the $\mathrm{MinE}^{D45A/V49A}$ mutant. In wild-type cells, MinD nucleates and grows rapidly until MinE caps it, switching it from a growing state to a shrinking state, analogous to microtubule catastrophe. When E-ring formation is prohibited in the $\mathrm{MinE}^{D45A/V49A}$ mutant, distinct growth and shrinking states are suppressed being replaced by interspersed addition and removal of monomers. The corresponding change in time scales of complete assembly and disassembly leaves enough time for the formation of a polar Z-ring thereby causing minicelling. Restated, this means that E-ring-dependent "dynamic instability" of the MinD polymers accelerates the cycle of polar Z-ring suppression thereby

preventing minicelling. This observation demonstrates that dynamic instability is not an isolated trick discovered by tubulin but is a general design principle employed by non-homologuous systems to carry out time-sensitive tasks.

Cooperativity provides robustness in the face of stochasticity.
Cooperativity has been reported in both MinD polymer formation and MinE induced hydrolysis (11, 29, 32). The exact role played by cooperativity *in vivo* is not clear. In the deterministic model, when stochasticity of MinD polymer nucleation and E-ring formation are introduced, they perturb the regularity of the oscillations but the perturbation is not severe provided cooperativity is present. The robustness of the oscillations can thus be interpreted to be at least in part due to the cooperativity of multi-stranded polymer nucleation. This relationship between stochasticity and cooperativity has been demonstrated previous for other biological system, for example, in regulation of the PER protein in circadian rhythms (54).

Experiments and predictions
The model provides predictions for phenotypes that have not been previously observed or have not been subject to quantification and also suggests several experiments. We describe some of these here.

Zhou et al. (2005) showed that mutations of MinD's α-helix α-7 (the yellow helix in Figure 3) did not prevent MinE from binding to MinD despite its inability to induce hydrolysis suggesting the presence of another binding domain. $\mathrm{MinE}^{D45A/V49A}$ was unable to form E-rings suggesting, as assumed in this paper, that the TS residues are involved in binding to MinD. Is MinE^{32-88} capable of binding to MinD? If so, is the binding sensitive to mutations in residues 45 and 49 of MinE?

The α-5 and α-6 domains of MinD are α-helices that are exposed on the face of MinD that is directly opposite its membrane-binding domain (α-11). They are also situated beside α-7, the domain thought to bind to MinE's anti-MinD domain (50). These domains are the most likely candidates for interaction with the TS residues of MinE. If MinE^{32-88} binds to MinD, is the binding sensitive to mutation of residues that lie in these domains?

In cells expressing the truncated protein MinE^{1-22}, does MinD behave similarly to what is seen in cells expressing $\mathrm{MinE}^{D45A/V49A}$? In either of these cells, does quantitative measurement of MinD helix dynamics agree with a random walk model for the polymer tip? As mentioned in the Results section, the random walk is biased, being driven to a polymer length that corresponds to a cytosolic concentration $D = k_{off}E/k_{on}$. This gives a prediction that the average polymer length is a linearly decreasing function of the expression level of MinE^{1-22} (or $\mathrm{MinE}^{D45A/V49A}$).

Over-expression of MinD by a factor of 2-3 in the *minE*$^-$ mutant should cause polymer nucleation at random along the cell membrane, similar to the phenotype of the phosphatidylethanolamine mutant (26) but more rapidly than seen in that context. This prediction is based on the estimate for the threshold membrane concentration of MinD calculated in the Appendix.

5 Appendix

Strain in membrane-bound MinD dimers In tubulating vesicles, MinD does work, the energy for which ultimately derives from the high energy ATP-bound state of MinD and is stored in strain energy in the membrane-bound dimer. This strain energy is used to overcome the activation energy for hydrolysis and so when strain is not maintained, the hydrolysis rate is slowed. By calculating the energy per monomer required to tubulate a vesicle of a particular size, we get a lower bound on the energy that can be stored in a strained MinD dimer.

Consider a vesicle of radius $R_0 = 400$ nm being deformed as shown in Figure 2. When a tube of length $l = 400$ nm and radius $r = 25$ nm is extracted from the vesicle, the osmotic pressure and the membrane surface tension equilibrate determining the overall volume contained within. The equation for mechanical equilibrium of this partially tubulated vesicle is

$$\frac{2}{R}K_s\frac{A-A_0}{A_0} = p_0\left(\frac{V_0}{V}-1\right)$$

where $A = 4\pi R^2 + 2\pi rl$ is the total surface area of the deformed vesicle, A_0 is the undeformed surface area, $V = 4/3\pi R^3 + \pi r^2 l$ is the total volume of the deformed vesicle, V_0 is the undeformed volume, $p_0 = 9.4 \cdot 10^7 k_B T/\mu m^3$ is the osmotic pressure of the buffer (estimated from the Methods section of (11)), $K_s = 4 \cdot 10^7 k_B T/\mu m^3$ is the membrane stretching modulus (55) and R is the radius to which the spherical portion of the vesicle equilibrates. Given any value of l, a value of R can be found and from that, the energy stored in stretching the membrane can be calculated: $E = \frac{K_s}{2}\frac{(A-A_0)^2}{A_0}$. The difference in energy between a vesicle with a tube of length $l = 400$nm and $l = 406$nm, which corresponds to the addition of 25 dimers, is $181k_BT$ or $7.2k_BT$ per dimer.

Strain in membrane-bound MinD dimers can dramatically bias MinD polymer nucleation to the poles

Denote the concentration of cytosolic MinD dimers by C (in number per μm^3), non-polar membrane-bound MinD dimers by M (number per μm^2), polar membrane-bound MinD dimers by P (number per μm^2) and cytosolic MinE dimers by E (μM)). Denote the surface area of the poles, upon which attached dimers are not strained, by A and the rest of the membrane surface area by $A_{tot} - A$ (in μm^2) . Suppose dimers associate to the non-polar membrane at a rate k_+CV where k_+ is the association rate constant (in units $1/(s\ \mu\text{m}^2)$) and dissociate from it at a rate $(k_-E + k_-^{bg})M$ where k_-^{bg} is the background release rate constant (in units $(1/s)$ and k_- is the MinE triggered release rate constant (in units $1/(s\ \mu\text{M})$). Similarly, at the poles, dimers associate at a rate $k_+\alpha CV$ where $\alpha =$ 2-9 is a factor accounting for a dimer preference for anionic lipids and dissociate at a rate $(k_-e^{-\Delta G}E + k_-^{bg})P$ where $\Delta G \sim 7$. The fact that the exponential factor multiplies the MinE rate but not k_-^{bg} reflects the necessary assumption that only the MinE induced hydrolysis rate and not the background rate is strain-dependent. If the background rate is also strain-dependent, this argument can explain polar accumulation of dimers but not the *minE*$^-$ mutant.

Setting these pairs of rates to be equal, the steady state concentrations can be found:

$$C = \frac{D_{tot}}{1 + \frac{k_+ \alpha A}{k_- e^{-\Delta G} E + k_{bg}} + \frac{k_+ (A_{tot} - A))}{k_- E + k_{bg}}},$$

$$P = \frac{k_+ \alpha C V}{k_- e^{-\Delta G} E + k_{bg}}, \quad M = \frac{k_+ C V}{k_- E + k_{bg}}.$$

In the presence of MinE, the ratio of polar to non-polar concentrations is

$$\frac{P}{M} = \alpha \frac{k_- E + k_{bg}}{k_- e^{-\Delta G} E + k_{bg}} = \alpha \frac{1 + \frac{k_{bg}}{k_- E}}{e^{-\Delta G} + \frac{k_{bg}}{k_- E}} \sim \alpha \frac{k_- E}{k_{bg}}.$$

where the approximation in the last step requires $e^{-\Delta G} << \frac{k_{bg}}{k_- E} << 1$. Hu and Lutkenhaus (2001) found that in the concentration range in which MinD forms polymers, the ratio of MinE induced to background hydrolysis is about 10. It is possible that given the restricted access to α-7 in polymerized form, this ratio is even greater for dimers. In either case, the approximation is valid. As a "worst case scenario", we take $\frac{k_- E}{k_{bg}} \sim 10$ and $\alpha = 2$. The dimer concentrations would be

$$C \sim 35 \text{ dimers}/\mu\text{m}^3, \quad P \sim 950 \text{ dimers}/\mu\text{m}^2, \quad M \sim 45 \text{ dimers}/\mu\text{m}^2.$$

In the absence of MinE ($E = 0$), the concentrations of MinD dimers at the poles and elsewhere are much closer, a fact interpreted in the Results section. Concentrations in this case are:

$$C_0 \sim 10 \text{ dimers}/\mu\text{m}^3, \quad P_0 \sim 250 \text{ dimers}/\mu\text{m}^2, \quad M_0 \sim 125 \text{ dimers}/\mu\text{m}^2.$$

A dimer-dimer dissociation constant somewhere between $P_0 = 250$ dimers/μm^2 and $P = 950$ dimers/μm^2 would simultaneously explain wild-type polar nucleation and the failure to form polar helices in the *minE*$^-$ mutant. This range is consistent with *in vitro* estimates of $D_{thresh} = 1.5 - 3\mu$M (11) which would correspond to a dimer-dimer dissociation constant range of 250-500 dimers/μm^2. A prediction emerging from this calculation is that intermediate levels of MinD over-expression in the *minE*$^-$ mutant should lead to polymer nucleation at the poles and possibly elsewhere on the membrane at high enough expression levels.

This calculation gives some insight into the rate of polymer nucleation. Dimer concentration on the membrane is proportional to the square of the cytosolic monomer concentration, D^2. If the dominant nucleation pathway was via a cytosolic monomer attaching to a membrane bound dimer, the nucleation rate would be proportional to D^3. However, the cytosolic monomer concentration is predicted to be quite low (35 dimers/μm^3). Thus, the more likely scenario is that nucleation proceeds by membrane-bound dimer-dimer binding and hence a cooperativity exponent of $n = 4$. However, for the simulations we used the more conservative exponent, $n = 3$.

MinD forms a double-stranded polymer

To address the question of the ultrastructure of the MinD polymer, we calculate the fraction of the cell can be wrapped by a MinD helix as a function of the presumed structure of the polymer given available estimates from the literature for the relevant biophysical parameters. The calculation indicates that a double-stranded is the most likely arrangement for a MinD polymer. It also suggests that the MinD helix is formed of a single two-stranded polymer that extends from pole to midcell.

The maximum possible length of a polymer is $L = N_D\delta/n$ where N_D is the total number of monomers available, δ is the size of a monomer and n is the number of strands in the polymer. The MinD polymer forms a helix with an angle of approximately $\theta = 80^\circ$ relative to the long axis of the cell (measured from images in (9)) so the length of the polymer projected onto that axis of the cell is $L_p = L\cos\theta$. As a fraction of the length of the cell (l), the projected length can be expressed as $f = L_p/l = 600c\pi r^2\delta\cos\theta/n$ where c is the total concentration of MinD, and r is the radius of the cylindrical cell. Provided the concentration of MinD is regulated so as not to change as a cell grows, this maximal-length covering-fraction is independent of cell length. Based on estimates extracted from the literature, $c \sim 4\mu$M (34, 48), $r \sim 0.35 - 0.5\mu$m (8), $\delta \sim 5$ nm (29) and $\theta \sim 80^\circ$ (9), it is clear that for $n = 2$ the maximal covering-fraction is reasonable ($f = 0.4 - 0.8$) and for $n = 3$, a maximum length polymer would barely be capable of reaching midcell ($f = 0.25 - 0.55$). For $n = 4$ (or greater), there is insufficient MinD to cover more than 40% of the cell's length. Due to the general prediction of short lengths for single-stranded polymers (30), $n = 1$ is also unlikely, requiring a polymer-tip dissociation constant of $10^{-5}\mu$M to achieve sufficient lengths. Although by this counting argument, a three-stranded polymer is marginally possible, a two-stranded model is the most consistent with the dimer structure of MinD (37) and with the electron microscopy observations of Suefuji et al. (2002).

Solution to model equations

Suppose the left MinD polymer is of length l_0 at $t = 0$ with an E-ring of full length l_{E_0}, and no polymer is present at the right pole. The length as a function of time, until complete disassembly, is

$$l(t) = -\beta t + l_0,$$

where $\beta = \delta k_{off}/2$. A polymer nucleates at the right pole when $D(t_{nuc}) \equiv D_{tot} - \gamma l(t_{nuc}) = D_{thresh}$ where $\gamma = 2/(600V\delta)$. Thus, the nucleation time is

$$t_{nuc} = \frac{l_0}{\beta} - \frac{D_{tot} - D_{thresh}}{\beta\gamma}.$$

Assuming $k_{on}D_{tot} >> k_{off}$ (polymerization is fast), the right polymer quickly equilibrates to length

$$r(t) = \frac{D_{tot}}{\gamma} + \beta t - l_0,$$

an expression valid from t_{nuc} until the polymer is capped. Capping on the right occurs when the

left E-ring disassembles to the point that the cytosolic concentration rises to E_{thresh}. Disassembly begins when $l(t) = l_{E_0}$ from which point the length of the E-ring is the same as the length of the MinD polymer. E-threshold is reached when $E(t_{cap}) \equiv E_{tot} - \gamma l(t_{cap}) = E_{thresh}$ which occurs at

$$t_{cap} = \frac{l_0}{\beta} - \frac{E_{tot} - E_{thresh}}{\beta\gamma}.$$

The length of the right polymer upon getting capped is

$$r(t_{cap}) = \frac{D_{tot} - (E_{tot} - E_{thresh})}{\gamma}.$$

Assigning this value to the initial length of the left polymer as well means that t_{cap} is also the half-period of the oscillation. Thus, the period of the oscillation is given by

$$T = 2\ \frac{D_{tot} - 2(E_{tot} - E_{thresh})}{\beta\gamma}.$$

The oscillatory solution exists provided a nucleated polymer is not capped immediately upon forming: $t_{nuc} < t_{cap}$. This reduces to the condition

$$D_{tot} - D_{thresh} > E_{tot} - E_{thresh}.$$

Parameter estimation

Parameter values in Table 6 with sources quoted as a citation only were found explicitly in the cited reference. "Estimated from" indicates that values were implicit and some calculations were required. Values for k_{off}, k_{on} and k_{on}^E were estimated from sequences of fluorescence images showing the temporal progression of the oscillations. k_{on} and k_{on}^E were taken simply so as to be as fast or faster than k_{off} as the latter parameter alone sets the time scale of the system. D_{tot} and E_{tot} were calculated from published estimates for the number of MinD and MInE monomers per cell $(34, 48)$ divided with estimates of cell volume. The pitch of the MinD helix, θ, was estimated from fluorescence images in (9) by measuring and averaging cell aspect ratios and number of apparent wraps from several images. The estimate of $\theta = 80^\circ$ was confirmed by generating helices of various angles as in Figure 5 and convolving with a Guassian PSF. Visual inspection ruled out angles less than about 77°.

In the stochastic implementation, $(\{n = 3, m = 3\})$ for the parameters k_{nuc} and k_{cap}, all values within the given range were tested and demonstrated oscillations. At the edges of the ranges, qualitative similarities to what is seen experimentally gradually break down, with delayed or overly rapid nucleation and/or E-ring formation as well as skipped beats occurring often. Values used for the trace in Figure 5 were $k_{nuc} = 0.006\mu\text{M}^{-3}\ \text{sec}^{-1}$ and $k_{cap} = 0.4\mu\text{M}^{-3}\ \text{sec}^{-1}$.

Diffusion and ADP-ATP exchange are two processes that have been invoked as crucial elements in various models in the literature. Due to the time scales associated with each of them, we have assumed they occur on time scales sufficiently fast that they can safely be assumed to be in

quasi-steady state. The cytosolic diffusion coefficient of both MinD and MinE has been previously estimated to be no smaller than $\mathcal{D} = 2.5\mu\text{m}^2/s$ in previous models. As MinD might spend some fraction of its time membrane-bound during the transit from one pole to the other, diffusion might be slowed by as much as an order of magnitude (56) in which case the effective diffusion would be $f_{cyto}\mathcal{D}_{cyto} + f_{memb}\mathcal{D}_{memb}$ where f_x is the fraction of time spent in either the cytosol or membrane bound. However, f_{memb} is likely small due to the rapid rates of hydrolysis, both MinE-induced (80/sec) and background ($\sim$ 8/sec – an order of magnitude smaller (7) but still significant). The time constant for such a diffusion coefficient in a cell 2-3 μm in length is $L^2/(2D) \sim$ 1-2 seconds.

The time scale for ADP-ATP exchange is not known for MinD but previous models have assumed a value around 1-2 seconds (17, 57–59) and others have either implicitly or explicitly assumed it to be rapid relative to other processes (14–16, 31, 60). Given that the time from onset of disassembly at one pole to nucleation at the other pole is necessarily less than the time required for Z-ring formation ($\sim$ 30 seconds) and requires at least one exchange per MinD monomer, the ADP-ATP exchange rate must be at least that fast. Provided the time constant for exchange is less than 10 sec (roughly the minimum time between disassembly onset and nucleation), it would not influence the dynamics of the model significantly.

6 Acknowledgments

The authors would like to acknowledge L.R. DeBella, L. Edelstein-Keshet and A. Mogilner for valuable feedback on the manuscript and P. Fletcher for help with generating figures. ENC is supported by funding from NSERC and MITACS and BM was funded through the NSERC-USRA summer program.

References

1. Margolin, W. 2005. Ftsz and the division of prokaryotic cells and organelles. *Nat Rev Mol Cell Biol.* 6:862–871.
2. Yu, X., and W. Margolin. 1999. Ftsz ring clusters in min and partition mutants: role of both the min system and the nucleoid in regulating ftsz ring localization. *Mol Microbiol.* 32:315–326.
3. de Boer, P., R. Crossley, and L. Rothfield. 1992. Roles of minc and mind in the site-specific septation block mediated by the mincde system of escherichia coli. *J Bacteriol.* 174:63–70.
4. Hu, Z., A. Mukherjee, S. Pichoff, and J. Lutkenhaus. 1999. The minc component of the division site selection system in escherichia coli interacts with ftsz to prevent polymerization. *Proc Natl Acad Sci USA.* 96:14819–14824.
5. de Boer, P., R. Crossley, and L. Rothfield. 1989. A division inhibitor and a topological specificity factor coded for by the minicell locus determine proper placement of the division septum in e. coli. *Cell.* 56:641–649.

6. Raskin, D., and P. de Boer. 1999. Minde-dependent pole-to-pole oscillation of division inhibitor minc in escherichia coli. *J Bacteriol*. 181:6419–6424.

7. Hu, Z., and J. Lutkenhaus. 2001. Topological regulation of cell division in e. coli. spatiotemporal oscillation of mind requires stimulation of its atpase by mine and phospholipid. *Mol Cell*. 7:1337–1343.

8. Raskin, D., and P. de Boer. 1999. Rapid pole-to-pole oscillation of a protein required for directing division to the middle of escherichia coli. *Proc Natl Acad Sci USA*. 96:4971–4976.

9. Shih, Y., T. Le, and L. Rothfield. 2003. Division site selection in escherichia coli involves dynamic redistribution of min proteins within coiled structures that extend between the two cell poles. *Proc Natl Acad Sci USA*. 100:7865–7870.

10. Raskin, D., and P. de Boer. 1997. The mine ring: an ftsz-independent cell structure required for selection of the correct division site in e. coli. *Cell*. 91:685–694.

11. Hu, Z., E. Gogol, and J. Lutkenhaus. 2002. Dynamic assembly of mind on phospholipid vesicles regulated by atp and mine. *Proc Natl Acad Sci USA*. 99:6761–6766.

12. Fu, X., Y. Shih, Y. Zhang, and L. Rothfield. 2001. The mine ring required for proper placement of the division site is a mobile structure that changes its cellular location during the escherichia coli division cycle. *Proc Natl Acad Sci USA*. 98:980–985.

13. Hale, C., H. Meinhardt, and P. de Boer. 2001. Dynamic localization cycle of the cell division regulator mine in escherichia coli. *EMBO J*. 20:1563–1572.

14. Meinhardt, H., and P. de Boer. 2001. Pattern formation in escherichia coli: a model for the pole-to-pole oscillations of min proteins and the localization of the division site. *Proc Natl Acad Sci USA*. 98:14202–14207.

15. Howard, M., A. Rutenberg, and S. de Vet. 2001. Dynamic compartmentalization of bacteria: accurate division in e. coli. *Phys Rev Lett*. 87:278102.

16. Kruse, K. 2002. A dynamic model for determining the middle of escherichia coli. *Biophys J*. 82:618–627.

17. Huang, K., Y. Meir, and N. Wingreen. 2003. Dynamic structures in escherichia coli: spontaneous formation of mine rings and mind polar zones. *Proc Natl Acad Sci USA*. 100:12724–12728.

18. Howard, M., and K. Kruse. 2005. Cellular organization by self-organization: mechanisms and models for min protein dynamics. *J Cell Biol*. 168:533–536.

19. Rodionov, V., and G. Borisy. 1997. Self-centring activity of cytoplasm. *Nature*. 386:170–173.

20. Cytrynbaum, E., V. Rodionov, and A. Mogilner. 2004. Computational model of dynein-dependent self-organization of microtubule asters. *J Cell Sci*. 117:1381–1397.

21. Malikov, V., E. Cytrynbaum, A. Kashina, A. Mogilner, and V. Rodionov. 2005. Centering of a radial microtubule array by translocation along microtubules spontaneously nucleated in the cytoplasm. *Nat Cell Biol*. 7:1113–1118.

22. Zheng, Y., M. Wong, B. Alberts, and T. Mitchison. 1995. Nucleation of microtubule assembly by a gamma-tubulin-containing ring complex. *Nature*. 378:578–583.

23. Machesky, L., S. Atkinson, C. Ampe, J. Vandekerckhove, and T. Pollard. 1994. Purification of a cortical complex containing two unconventional actins from acanthamoeba by affinity chromatography on profilin-agarose. *J Cell Biol*. 127:107–115.

24. Norris, V., C. Woldringh, and E. Mileykovskaya. 2004. A hypothesis to explain division site selection in escherichia coli by combining nucleoid occlusion and min. *FEBS Lett*. 561:3–10.

25. Mileykovskaya, E., and W. Dowhan. 2000. Visualization of phospholipid domains in escherichia coli by using the cardiolipin-specific fluorescent dye 10-n-nonyl acridine orange. *J Bacteriol*. 182:1172–1175.

26. Mileykovskaya, E., I. Fishov, X. Fu, B. Corbin, W. Margolin, and W. Dowhan. 2003. Effects of phospholipid composition on mind-membrane interactions in vitro and in vivo. *J Biol Chem*. 278:22193–22198.

27. Rowland, S., X. Fu, M. Sayed, Y. Zhang, W. Cook, and L. Rothfield. 2000. Membrane redistribution of the escherichia coli mind protein induced by mine. *J Bacteriol*. 182:613–619.

28. Lipowsky, R., and R. Dimova. 2003. Domains in membranes and vesicles. *Journal of Physics: Condensed Matter*. 15:S31–S45.

29. Suefuji, K., R. Valluzzi, and D. RayChaudhuri. 2002. Dynamic assembly of mind into filament bundles modulated by atp, phospholipids, and mine. *Proc Natl Acad Sci USA*. 99:16776–16781.

30. Howard, J. 2001. Mechanics of Motor Proteins and the Cytoskeleton. Sinauer Associates, Inc, Sunderland, Massachusetts.

31. Drew, D., M. Osborn, and L. Rothfield. 2005. A polymerization-depolymerization model that accurately generates the self-sustained oscillatory system involved in bacterial division site placement. *Proc Natl Acad Sci USA*. 102:6114–6118.

32. Lackner, L., D. Raskin, and P. de Boer. 2003. Atp-dependent interactions between escherichia coli min proteins and the phospholipid membrane in vitro. *J Bacteriol*. 185:735–749.

33. Hu, Z., C. Saez, and J. Lutkenhaus. 2003. Recruitment of minc, an inhibitor of z-ring formation, to the membrane in escherichia coli: role of mind and mine. *J Bacteriol*. 185:196–203.

34. de Boer, P., R. Crossley, A. Hand, and L. Rothfield. 1991. The mind protein is a membrane atpase required for the correct placement of the escherichia coli division site. *EMBO J*. 10:4371–4380.

35. Zhang, Y., S. Rowland, G. King, E. Braswell, and L. Rothfield. 1998. The relationship between hetero-oligomer formation and function of the topological specificity domain of the escherichia coli mine protein. *Mol Microbiol*. 30:265–273.

36. Szeto, T., S. Rowland, L. Rothfield, and G. King. 2002. Membrane localization of mind is mediated by a c-terminal motif that is conserved across eubacteria, archaea, and chloroplasts. *Proc Natl Acad Sci USA*. 99:15693–15698.

37. Hu, Z., and J. Lutkenhaus. 2003. A conserved sequence at the c-terminus of mind is required for binding to the membrane and targeting minc to the septum. *Mol Microbiol*. 47:345–355.

38. Lutkenhaus, J., and M. Sundaramoorthy. 2003. Mind and role of the deviant walker a motif, dimerization and membrane binding in oscillation. *Mol Microbiol*. 48:295–303.

39. Sweitzer, S., and J. Hinshaw. 1998. Dynamin undergoes a gtp-dependent conformational change causing vesiculation. *Cell*. 93:1021–1029.

40. Fygenson, D., J. Marko, and A. Libchaber. 1997. Mechanics of microtubule-based membrane extension. *Phys Rev Lett*. 79:44974500.

41. Bo, L., and R. Waugh. 1989. Determination of bilayer membrane bending stiffness by tether formation from giant, thin-walled vesicles. *Biophys J*. 55:509–517.

42. Fournier, L., and B. Joos. 2003. Lattice model for the kinetics of rupture of fluid bilayer membranes. *Phys Rev E Stat Nonlin Soft Matter Phys*. 67:051908.

43. Edelstein-Keshet, L., and G. Ermentrout. 1998. Models for the length distributions of actin filaments: I. simple polymerization and fragmentation. *Bull Math Biol*. 60:449–475.

44. Fygenson, D., H. Flyvberg, K. Sneppen, A. Libchaber, and S. Leibler. 1995. Spontaneous nucleation of microtubules. *Phys Rev E Stat Nonlin Soft Matter Phys*. .

45. Zhao, C., P. de Boer, and L. Rothfield. 1995. Proper placement of the escherichia coli division site requires two functions that are associated with different domains of the mine protein. *Proc Natl Acad Sci USA*. 92:4313–4317.

46. Pichoff, S., B. Vollrath, C. Touriol, and J. Bouche. 1995. Deletion analysis of gene mine which encodes the topological specificity factor of cell division in escherichia coli. *Mol Microbiol*. 18:321–329.

47. King, G., Y. Shih, M. Maciejewski, N. Bains, B. Pan, S. Rowland, G. Mullen, and L. Rothfield. 2000. Structural basis for the topological specificity function of mine. *Nat Struct Biol*. 7:1013–1017.

48. Shih, Y., X. Fu, G. King, T. Le, and L. Rothfield. 2002. Division site placement in e.coli: mutations that prevent formation of the mine ring lead to loss of the normal midcell arrest of growth of polar mind membrane domains. *EMBO J*. 21:3347–3357.

49. Zhou, H., R. Schulze, S. Cox, C. Saez, Z. Hu, and J. Lutkenhaus. 2005. Analysis of mind mutations reveals residues required for mine stimulation of the mind atpase and residues required for minc interaction. *J Bacteriol*. 187:629–638.

50. Ma, L., G. King, and L. Rothfield. 2004. Positioning of the mine binding site on the mind surface suggests a plausible mechanism for activation of the escherichia coli mind atpase during division site selection. *Mol Microbiol*. 54:99–108.

51. Szeto, J., N. Eng, S. Acharya, M. Rigden, and J. Dillon. 2005. A conserved polar region in the cell division site determinant mind is required for responding to mine-induced oscillation but not for localization within coiled arrays. *Res Microbiol*. 156:17–29.

52. Hayashi, I., T. Oyama, and K. Morikawa. 2001. Structural and functional studies of mind atpase: implications for the molecular recognition of the bacterial cell division apparatus. *EMBO J.* 20:1819–1828.

53. Holy, T., and S. Leibler. 1994. Dynamic instability of microtubules as an efficient way to search in space. *Proc Natl Acad Sci USA*. 91:5682–5685.

54. Gonze, D., J. Halloy, and A. Goldbeter. 2002. Robustness of circadian rhythms with respect to molecular noise. *Proc Natl Acad Sci USA*. 99:673–678.

55. Evans, E., and W. Rawicz. 1990. Entropy-driven tension and bending elasticity in condensed-fluid membranes. *Phys Rev Lett*. 64:2094–2097.

56. Alberts, B., D. Bray, J. Lewis, M. Raff, R. K, and W. JD. 1994. Molecular Biology of the Cell. Garland Publishing.

57. Kerr, R., H. Levine, T. Sejnowski, and W. Rappel. 2006. Division accuracy in a stochastic model of min oscillations in escherichia coli. *Proc Natl Acad Sci USA*. 103:347–352.

58. Fange, D., and J. Elf. 2006. Noise-induced min phenotypes in e. coli. *PLoS Comput Biol*. 2:e80.

59. Pavin, N., H. Paljetak, and V. Krstic. 2006. Min-protein oscillations in escherichia coli with spontaneous formation of two-stranded filaments in a three-dimensional stochastic reaction-diffusion model. *Phys Rev E Stat Nonlin Soft Matter Phys*. 73:021904.

60. Meacci, G., and K. Kruse. 2005. Min-oscillations in escherichia coli induced by interactions of membrane-bound proteins. *Phys Biol*. 2:89–97.

Table of Parameters

Parameter	Description	Value	Source
k_{off}	E-ring induced MinD hydrolysis/ dissociation rate	80 sec^{-1}	Estimated from (13).
k_{on}	MinD polymerization rate constant	100 μM^{-1} sec^{-1}	Estimated from (13).
k_{on}^{E}	E-ring elongation rate constant	160 μM^{-1} sec^{-1}	Estimated from (13).
k_{nuc}	MinD polymer nucleation rate constant	0.001-0.1 μM^{-3} sec^{-1}	See text.
k_{cap}	E-ring initiation rate constant	0.06-1.5 μM^{-3} sec^{-1}	See text.
K_D	MinE dimer dissociation constant	0.6 μM^{-1}	(35).
D_{tot}	Total MinD concentration	4 μM	Estimated from (34, 48).
E_{tot}	Total MinE concentration	3 μM	Estimated from (48).
D_{thresh}	Threshold MinD concentration	1.5-3μM	(11).
E_{thresh}	Threshold MinE concentration	2.5 μM	Fitted parameter, see text.
δ	MinD monomer diameter	5 nm	(29).
L, V	Cell radius, volume	$\sim 1/2\mu$m, $\sim 1\mu\text{m}^3$	Typical dimensions.
θ	MinD helix pitch angle	80°	Estimated from (9).
λ	*minD* phage expression level	3.3 μM	Fitted parameter, see text.

Table 1: Parameters used in the deterministic and stochastic versions of the model.

Results of Fitting Parameter Values to Data

Genotype	Osc. period	Max. coverage
wild type	45 seconds (38 seconds)	40%
minD over-expression	94 seconds (96 seconds)	78%
minDE over-expression	20 seconds (34 seconds)	50%
minDE expression in $\Delta minCDE$	50 seconds (40 seconds)	38%

Table 2: Fitted oscillation periods and resulting maximal MinD coverage are given for each expression experiment. Experimentally measured values (8) are in parentheses. These data were fitted by a least squares method generating predictions for expression level, $\lambda = 3.3\mu$M, and E-ring-formation threshold, $E_{thresh} = 2.5\mu$M). This value of λ is low relative to wild-type levels.

Figure 1: Proposed dimer model. (A) MinE undergoes dimerization. Residues 45 and 49 are shown as light patches on the underside of the MinE dimer. (B) MinD cycles from the cytosol where it binds ATP (i), dimerizes (ii), attaches to the (flat) membrane taking on a strained conformation (iii), recruits MinE (iv), hydrolyzes ATP and is released from the membrane (v). If membrane attachment occurs in a region of low tension where MinD can easily deform the membrane or where the membrane is already curved (vi), the lack of strain in the dimer prevents hydrolysis and release (vii). This leads to an accumulation of dimers in such regions. MinE is proposed to undergo a conformation change in which the anti-MinD domain moves to the MinD dimerization face (v) simultaneously blocking polymerization of dimers and inducing MinD ATPase activity.

Figure 2: Progression of vesicle tubulation. (a) MinD binds to a slack vesicle, (b) begins to polymerize thereby pulling out any extra membrane and (c) eventually stretches the membrane as the membrane/polymer tube grows. In panel (b), the force $F \approx 0 - 3$ pN is opposed mostly by membrane bending. In (c), the force $F \approx 10$ pN is opposed by the membrane tension (T) which is assumed to be in mechanical equilibrium with the osmotic pressure (π) induced by volume change.

Figure 3: E-ring formation and function. (A) E-ring nucleation by two pathways: sequential monomer binding or dimer binding. The monomer pathway is less preferred than the dimer pathway due to the extra intermediate step. In either case, once MinE is attached at the tip, MinD is prevented from binding by the anti-MinD domain. (B) Top view of the MinD dimer structure proposed by Lutekenhaus and Sundaramoorthy (2003) superimposed on the cartoon shape of MinD. ATP are in dark gray. The α-helices (α-4 and α-7) known to influence the anti-MinD activity of MinE are in green and yellow respectively (50, 51). Note how the α-4 and α-7 domains from opposite monomers come together when the dimer forms. The blue α-helix is present in the structure of the analogous ATPase NifH but is missing from MinD (38). We propose that the anti-MinD domain of MinE takes its place.

Figure 4: Approximate solution in the limit of rapid polymer growth. The exact solution differs only in the growth phase through which linear growth is replaced by an exponential approach to linear growth (dashed curve). The first polymer is capped at $t = 0$ and is only seen disassembling under the influence of the E-ring (dark shading). t_{nuc} denotes the time at which the first polymer tip crosses the nucleation threshold (long dashes) meaning that the cytosolic MinD concentration is sufficient to nucleate the second polymer. t_{dis} is the time at which the old E-ring begins disassembly. t_{cap} is the time at which the first polymer tip crosses the capping threshold meaning the cytosolic MinE concentration is sufficient to form a new E-ring on the second polymer. This process repeats with a period $T = 2t_{cap}$. Light shading represents the MinD polymer and hence the region in which Z-ring formation is inhibited.

Figure 5: Numerical solution to stochastic implementation. (A) A set of traces from one run of the stochastic simulation. Blue curves represent MinD polymers tips; blue shading represents MinD polymers; red dashed curves denote the growing end of the E-rings; red shading represents E-rings. (B) A sequence of images showing approximately one half period, generated from the traces in (A). Each frame corresponds to a dashed line in (A) (from 57 to 94.5 seconds in 7.5 second intervals). MinD polymer (blue circles, outlined), MinE ring (red, outlined), cytosolic MinD (blue, no outline), cytosolic MinE (red, no outline). For clarity, only half of the cytosolic MinD monomers, all cytosolic MinE dimers and one out of every eight monomers in polymer form are shown. Note that in the model, polymer lengths and (well-mixed) cytosolic concentrations are tracked as scalar quantities; for visualization only, spatial distribution in the cytosol is by uniform random placement and the helical shape is prescribed (consistent with measurements from the images of Shih et al. 2003). Frame 1: A pre-existing polymer is almost entirely disassembled (bottom). A new polymer (top) is growing. Note that cytosolic MinE dimer concentration is high and as a result E-ring formation will occur soon on the growing polymer. Frame 2: An E-ring has formed; MinE dimer concentration is low and remains low until Frame 5. Cytosolic MinD concentration is also low. Frame 3: Cytosolic MinD concentration rises as the upper polymer disassembles. Frame 4: The same trend continues. Frame 5: A MinD polymer has formed at the bottom and cytosolic MinE dimer concentration has begun to rise. Frame 6: Cytosolic MinE concentration has risen sufficiently to allow an E-ring to form on the lower polymer (equivalent to Frame 2, one half-period later).

Figure 6: Polymerization dynamics in three different types of theoretical cells. One cell with cooperative nucleation of MinD and cooperative capping by MinE (top), one with non-cooperative nucleation of MinD and cooperative capping by MinE (middle), and one with cooperative nucleation of MinD and non-cooperative capping by MinE (bottom). Notice the loss of regularity in the lower two panels.

Fig 1

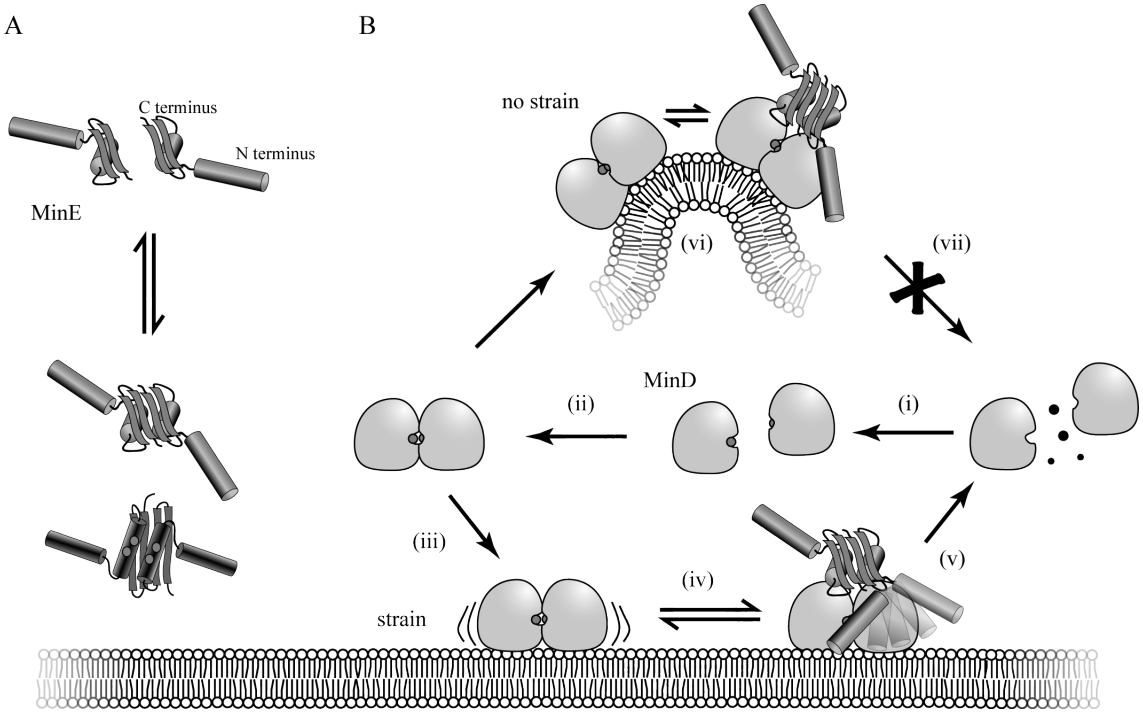
A
B
C terminus
N terminus
MinE
no strain
(vi)
(vii)
MinD
(ii)
(i)
(iii)
(iv)
(v)
strain

Fig 2

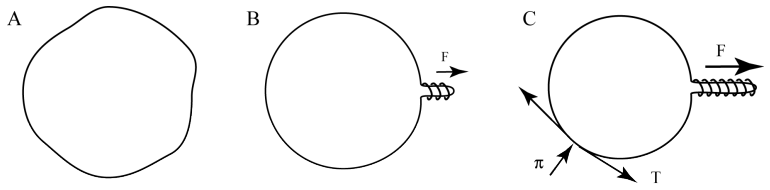

Fig 3

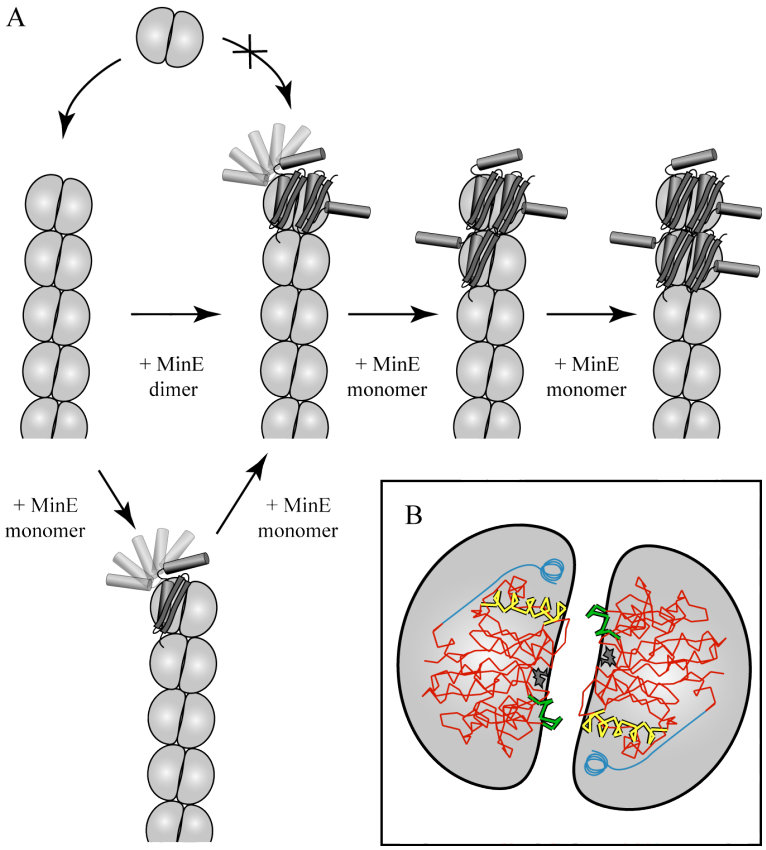
A
+ MinE
dimer
+ MinE
monomer
+ MinE
monomer
+ MinE
monomer
+ MinE
monomer
B

Fig 4

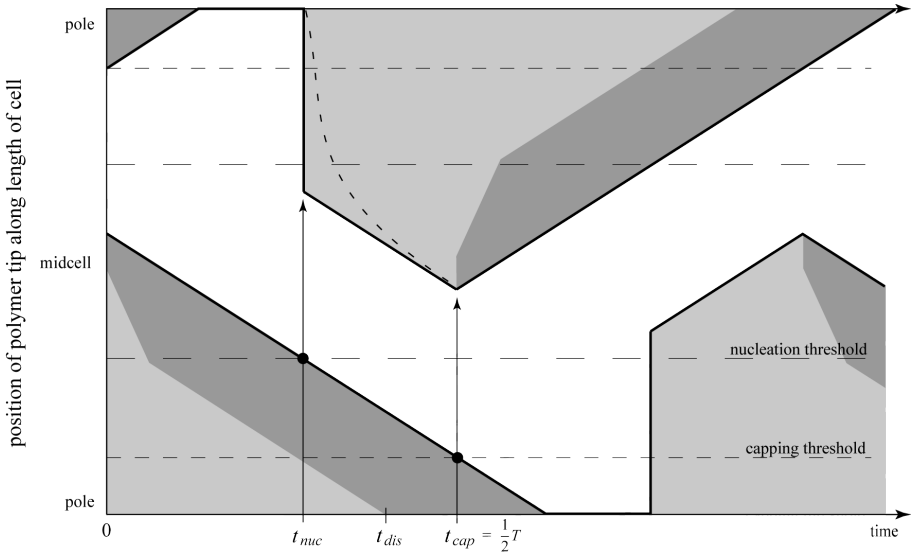
pole
midcell
pole
position of polymer tip along length of cell
nucleation threshold
capping threshold
0
t_{nuc}
t_{dis}
$t_{cap} = \frac{1}{2}T$
time

Fig 5

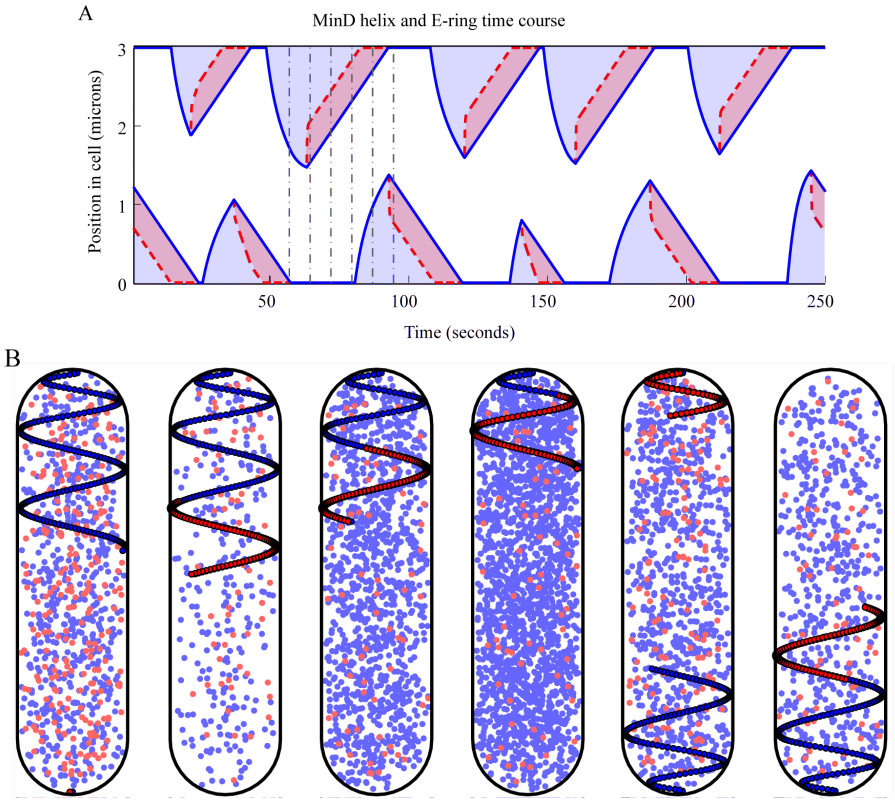
A
MinD helix and E-ring time course
Position in cell (microns)
0
1
2
3
50
100
150
200
250
Time (seconds)
B

Fig 6

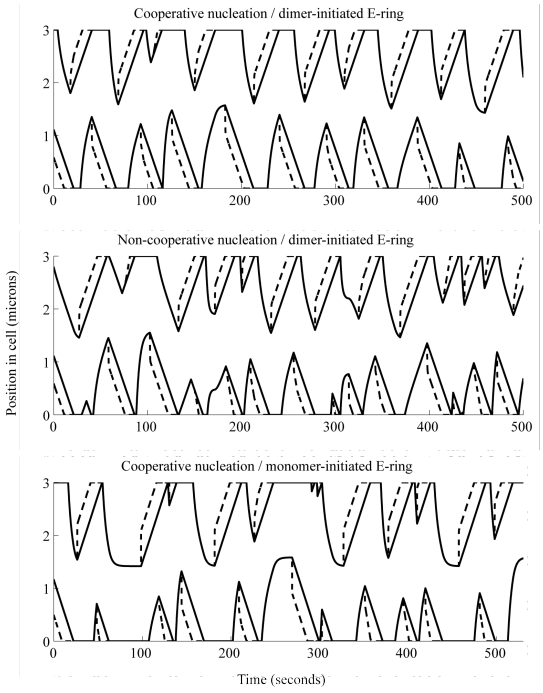
Cooperative nucleation / dimer-initiated E-ring
Non-cooperative nucleation / dimer-initiated E-ring
Cooperative nucleation / monomer-initiated E-ring
Position in cell (microns)
Time (seconds)
0
1
2
3
0
100
200
300
400
500